

# **Structural Tunability of Multicompartment Micelles as a Function of Lipophilic-Fluorophilic Block Length Ratio**

Connor P. Callaway<sup>1</sup>, Nicholas Bond<sup>1</sup>, Kayla Hendrickson<sup>1</sup>, Seung Min Lee<sup>1</sup>,  
and Seung Soon Jang<sup>1,2,3,4,\*</sup>

<sup>1</sup> Computational NanoBio Technology Laboratory, School of Materials Science and Engineering, Georgia Institute of Technology, 771 Ferst Drive NW, Atlanta, GA 30332-0245, USA

<sup>2</sup> Institute for Electronics and Nanotechnology, Georgia Institute of Technology, Atlanta, GA, USA

<sup>3</sup> Parker H. Petit Institute for Bioengineering and Bioscience, Georgia Institute of Technology, Atlanta, GA, USA

<sup>4</sup> Strategic Energy Institute, Georgia Institute of Technology, Atlanta, GA, 30332, USA

---

\*Corresponding author. Email address: [seungsoon.jang@mse.gatech.edu](mailto:seungsoon.jang@mse.gatech.edu)

## ABSTRACT

Structural variation in multicompartment micelles consisting of lipophilic-hydrophilic-fluorophilic (hereafter referred to as BAC) triblock copolymers is investigated using the dissipative particle dynamics simulation method. It is demonstrated from our results that the structure of BAC multicompartment micelles is effectively tuned as a function of the lipophilic-fluorophilic ratio parameter, here termed  $\mathcal{R}_l$ , of the constituent linear triblock copolymers. In particular, a morphological deviation from onion-like ABC micelles arises in BAC micelles systems as  $\mathcal{R}_l$  increases. The morphologies of BAC micelles with  $\mathcal{R}_l \ll 1$  or  $\mathcal{R}_l \gg 1$  display striking similarities, with the only notable difference being an inversion of the lipophilic and fluorophilic regions. When  $\mathcal{R}_l \approx 1$ , segmented worm-like structures with multiple cores are favored in BAC micelle systems. Through this study, it is confirmed that the block length ratio is an effective control parameter to tune the structure of multicompartment micelles.

## 1. INTRODUCTION

Efficient reaction design forms an important foundation of many processes in modern chemistry. Reaction optimization has far-reaching effects that greatly improve many other facets of polymer manufacturing, pharmaceutical production, and related industries<sup>1-8</sup>. In particular, the field of immobilized molecular catalysis has attracted particular interest in recent decades<sup>9-18</sup>. By allowing high selectivity and reaction rates traditionally achieved by homogeneous catalysis while still yielding the excellent separability offered by heterogeneous catalysis, this field presents an opportunity to leverage the advantages of both techniques<sup>19-24</sup>.

Despite the strengths of immobilized molecular catalysis, systems containing multiple *tandem* non-orthogonal reactions present significant difficulties<sup>25-28</sup>. Non-orthogonality in complex reaction processes introduces a challenge in designing for maximal reaction efficiency. Individual steps of a multistep reaction may be undesirably affected by other species present in the previous or next steps in the reaction<sup>29</sup>. In such cases, the catalyzing agent could suffer drastically reduced efficacy or cease to function altogether<sup>29-30</sup>.

A potential solution to these obstacles arises in a field of growing academic interest in recent years. Multicompartment micelles offer separate regions in which each of the non-orthogonal reactions can take place, allowing one-pot synthesis and tandem catalysis<sup>29, 31-35</sup>. Micelles are, of course, well studied in colloid chemistry; indeed, the *multicompartment* micelle (MCM) is simply an extension of the traditional idea. It is well known that a traditional micelle is composed of amphiphilic molecules which have hydrophilic and hydrophobic parts<sup>36-37</sup>. MCMs, then, are composed of polymers of three or more blocks of distinct solvophilicity.

Common examples result from triblock copolymers containing hydrophilic, lipophilic, and fluorophilic blocks<sup>38-43</sup>. By introducing immobilized catalysts into MCM systems, it is possible to

create a micelle *nanoreactor*<sup>44-48</sup>. Different catalysts may be attached to each block of the triblock copolymer; the immobilized catalysts are then confined to specific regions of the MCM. These distinct catalytic regions within the structure support simultaneous non-orthogonal reactions in the same chamber while still achieving high reaction rates and easy separability<sup>49-51</sup>.

The morphology of the micelles determined by a given block copolymer affects the utility of these micelles for nanoreactor applications. By extension, the architecture of the constituent triblock polymers has a marked effect on the performance of the resultant micelle nanoreactor system. For example, even if the different species in the triblock copolymer are held constant, variations in the sequence, lengths, and length ratios of the respective blocks can lead to significant morphological changes in the resultant MCMs<sup>41-43, 52</sup>. These changes can lead to decreased extent of compartmentalization (leading to diminished catalyst effectiveness) or less efficient transport of reactant and product (leading to reduced reaction rates).

In order to offer larger control over these effects, the present work aims to identify a key parameter which may be easily modified during polymer synthesis and which leads to significant MCM structural tunability. Identifying such a useful experimental parameter in turn allows for more effective control of reactant and product transport through the micelle, offering improved nanoreactor capability. The results presented here show that simply by varying the lipophilic-to-fluorophilic block length ratio, a spectrum of morphologies may be generated.

Using coarse-grained molecular dynamics, this study examines the effects of triblock copolymer architecture on aqueous MCM morphology in both hydrophilic-lipophilic-fluorophilic (hereafter ABC) systems and lipophilic-hydrophilic-fluorophilic (BAC) systems. Through the dissipative particle dynamics simulation method<sup>53-56</sup>, a significant structural difference between ABC and BAC micelle systems are studied. Following this, a more detailed study of the BAC

system uncovers a morphological trend which highlights the dependence of the micelle structure on the lipophilic-to-fluorophilic block length ratio.

## 2. MODELING AND SIMULATION METHODS

The self-assembled micelle structures formed by a triblock copolymer in solution can vary quite widely, even though the chemical species within each block are unchanged<sup>41-43, 52, 57-60</sup>. Other variables associated with the architecture of the copolymer may drastically affect the resultant structures. A trivial example lies in the difference between ABC and BAC micelles in water, where blocks A, B, and C are taken to represent hydrophilic, lipophilic, and fluorophilic blocks, respectively.

The micelle structures formed by ABC triblock copolymers have been studied quite extensively<sup>52, 57-58, 61-62</sup>. These polymers readily form layered spheroids (referred to as “onion” morphologies<sup>63-67</sup>) composed of a fluorophilic core, an intermediate lipophilic layer, and a hydrophilic corona. If, however, the block sequence is modified to BAC, more exotic morphologies may easily be formed depending on the triblock copolymer block lengths.

In this study, dissipative particle dynamics (DPD) is used through Materials Studio<sup>68</sup> to examine the effect of the lipophilic-fluorophilic block length ratio on the resultant MCM morphology within both ABC and BAC systems. We define this ratio for a *purely linear* chain as

$$\mathcal{R}_l = \tilde{b}_L / \tilde{b}_F, \tag{1}$$

where  $\tilde{b}_L$  and  $\tilde{b}_F$  represent the reduced DPD block lengths corresponding to a real polymer of lipophilic and fluorophilic block lengths  $b_L$  and  $b_F$ . The variation in micelle structure as a function of  $\mathcal{R}_l$  is studied at several fixed hydrophilic block lengths.

Based on the favorability of contributions from bulk interactions to the reduction of total energy, three morphological regimes are predicted to arise based on the  $\mathcal{R}_l$ -value of the constituent triblock copolymer. For  $\mathcal{R}_l$ -values either much greater than or much less than unity, it is expected that volume free energy contributions of the excess species with higher  $\tilde{b}$ -value will dominate, leading to the formation of spheroidal micelles with a lipophilic core (if  $\mathcal{R}_l \gg 1$ ) or fluorophilic core (if  $\mathcal{R}_l \ll 1$ ). The core is covered by patches of the species with the lower  $\tilde{b}$ -value and finally a hydrophilic corona.

By contrast, for  $\mathcal{R}_l$  near unity, it is predicted that a single-cored structure becomes less stable due to the competing volume free energy contributions arising from both the lipophilic and the fluorophilic species. Instead, polymers with  $\mathcal{R}_l$  near unity are expected to result in morphologies ranging from segmented worm-like structures to agglomerates of multiple cores.

For the DPD simulations performed in this study, the system was defined as 5% polymer and 95% water. This polymer concentration is larger than the one necessary in a real physical system; the larger concentration is chosen in our simulations to ensure a significant amount of polymer interactions. The simulation box size was defined to be  $30 \times 30 \times 30$  with grid spacing of 1.0 and a bead density of 3.0, allowing the use of the linear relationship between the Flory-Huggins  $\chi$ -parameter and the corresponding DPD repulsion parameter ( $a_{ij}$ ) for a given pair of molecular species<sup>56</sup>.

$$a_{ij} = 25 + 3.5\chi_{ij} \tag{2}$$

Total simulation time was generally taken to be  $\alpha t_e$ , where  $t_e$  is the minimum time required to achieve pressure equilibration. The constant  $\alpha$ , chosen arbitrarily to be equal to 2.5, allows the simulation to continue for a fixed amount of time after initially reaching the equilibration stage to ensure that the system is settled into a fully equilibrated state. A visual

representation of this equilibration is presented in Figure 1a. For a timestep of 0.05 reduced DPD unit, a total time of  $8.75 \times 10^3$  reduced DPD units was determined to be satisfactory for all simulations. The reduced DPD unit time is taken to be the amount of time necessary for a bead to diffuse a distance of its own radius due to thermal fluctuations<sup>55-56</sup>. It should be noted that choosing a timestep greater than 0.05 reduced unit is discouraged. As observed by Groot and Warren<sup>56</sup>, employing a timestep greater than this value results in artificial temperature increases in violation of equipartition. The physical soundness of the DPD simulation can be gauged by examining the variation in system temperature and system pressure over the entire simulation time, as shown in Figure 1.

The species A, B, and C are loosely based on the species displayed in Figure 2; these three species were selected for their spectrum of solvophilicity. Repulsion parameters for this study were assigned in order to ensure immiscibility between the A, B, and C blocks between both each other and water. The exact values were based first on  $\chi$ -values calculated via the COMputational Miscibility Analysis (COMMA) method previously introduced by the authors<sup>69</sup>, converted to repulsion parameters via equation (2), and finally adjusted in order to guarantee distinct three-phase separation upon self-assembly. Table 1 summarizes the values of these repulsion parameters. The *total* polymer length (i.e.,  $\tilde{b}_H + \tilde{b}_L + \tilde{b}_F$ ) was constrained to 27 in all simulations performed in this study to guarantee a maximum extended polymer length shorter than the simulation box size in all dimensions.

### 3. RESULTS AND DISCUSSION

As noted previously, it is expected that ABC micelles exhibit significantly less structural variation than the corresponding BAC micelles. Of course, this expectation is quite reasonable: the

onion-like shell structure often formed in ABC micelle systems minimizes unfavorable interactions by aligning the triblock copolymer chain according to its sequential change in hydrophilicity. In BAC micelle systems, however, the triblock copolymer generates a larger variety of structures to minimize the free energy, since the traditional layered structures are not always possible.

Indeed, simulation results bear out this prediction quite satisfactorily. Figure 3 displays the differences which arise between ABC and BAC micelle systems for  $\mathcal{R}_l$  less than, equal to, and greater than unity (with the reduced hydrophilic block length held constant at  $\tilde{b}_H = 15$ ). When the fluorophilic block is longer than the lipophilic block (i.e.,  $\mathcal{R}_l$  is less than unity), the ABC and BAC systems form nearly identical structures. As the  $\mathcal{R}_l$ -value approaches unity, however, the BAC system begins to diverge from a single-cored structure. In the limit as  $\mathcal{R}$  becomes much greater than unity, the fluorophilic block becomes the deficient species, which causes a significant structural change in the BAC system and a significant divergence between the two systems (Figures 3d and 3h). The ABC system displays no structural changes as a result of modifying  $\mathcal{R}_l$ ; an onion-like configuration is favored in each case. Increasing the  $\mathcal{R}_l$ -value in the ABC system corresponds only to generating a thicker lipophilic shell and a smaller fluorophilic core, while in the BAC system it causes a complete core inversion.

The difference between the two systems becomes quite pronounced in the limit of  $\mathcal{R}_l \gg 1$ . In fact, even when the hydrophilic block is shortened, ABC micelle systems still exhibit a dominant preference for fluorophilic-cored spheroidal micelles across all  $\mathcal{R}_l$ -values, as shown in Figure 4. BAC micelle systems, by contrast, again display a complete inversion of the ABC morphology for large  $\mathcal{R}_l$ , forming micelles with fluorophilic patches surrounding a lipophilic core.

These results demonstrate that ABC micelle systems are relatively insensitive to changes in the  $\mathcal{R}_l$ -value, instead forming characteristically onion-like structures independently of this

controlling parameter. When considering BAC micelle systems, however, modifying the  $\mathcal{R}_l$ -value leads to a wider range of micelle configurations. Indeed, as predicted previously, BAC micelle systems exhibit three distinct structural regimes based upon  $\mathcal{R}_l$ . Considering the lipophilic and fluorophilic blocks as the two competing species in determining the micelle configuration, when  $\mathcal{R}_l$  strongly deviates from unity in either direction, there is a strong tendency to form spheroidal micelles with a core composed of the excess species and patches of the deficient species. For  $\mathcal{R}_l$ -values close to unity, neither of the blocks forms a dominant core and segmented structures are favored over spheroidal structures. In all cases, the hydrophilic blocks form an outer shell around the micelle – curiously, there does not appear to be a governing structural pattern in the modification of  $\tilde{b}_H$ .

Simulation results for a series of BAC micelle systems as a function of  $\mathcal{R}_l$ -values are presented in Figure 5a, where the horseshoe-like shape highlights the structural similarities at either extreme of  $\mathcal{R}_l$ . For improved clarity, due to the thickness of the hydrophilic shell, visibility of the hydrophilic block is disabled in Figure 5b. Note that the reduced hydrophilic block length  $\tilde{b}_H = 18$  for all simulations in Figure 5.

It is clear that the preference for the formation of a strongly spheroidal morphology increases as  $\mathcal{R}_l$  becomes further from unity. Patches composed of the deficient species surround the core in these extremes (namely, regimes I and III). As  $\mathcal{R}_l$  approaches unity, however, these patches become larger; near  $\mathcal{R}_l = 1$ , the micelle structure becomes decidedly non-spheroidal (regime II). It is clear that segmented worm-like configurations arise for B<sub>4</sub>A<sub>18</sub>C<sub>5</sub> and B<sub>5</sub>A<sub>18</sub>C<sub>4</sub>. This behavior is especially evident in Figure 5b, where the hydrophilic block visibility is disabled.

As previously noted, the total polymer length was constrained to 27 in all cases. Due to this constraint, simulations with smaller  $\tilde{b}_H$  may take on larger values of  $\tilde{b}_L$  and  $\tilde{b}_F$  and

consequently have access to a wider range of  $\mathcal{R}_l$ -values. Based on Figure 5, then, it should be expected that BAC triblock copolymers with larger  $\mathcal{R}_l$ -values should have a stronger preference to form spheroidal structures upon self-assembly.

Indeed, results from simulations performed for  $\tilde{b}_H$ -values of 15, 12, and 9 clearly demonstrate increasingly spheroidal morphologies in the regime I and III limits (where  $\mathcal{R}_l$  is far from unity), as seen in the horseshoe diagrams in Figures 6-8. Micelles in the intermediate range between regimes I/III and II characteristically display patches of the deficient species (again, either lipophilic or fluorophilic) with the core comprised of the excess species. As an extension of the patches observed at intermediate  $\mathcal{R}_l$ , micelles in regime II display the predicted agglomerates composed of multiple similarly-sized cores of both lipophilic and fluorophilic species.

It bears noting that no predominant structural patterns arise as a result of the decrease in  $\tilde{b}_H$ . This value appears to correspond solely to the thickness of the hydrophilic shell which surrounds the micelle, rather than any direct morphological changes. Certainly there is no discernible pattern in regimes I and III. Moreover, any trend in regime II appears to be exceedingly minor if present at all. In fact, this observation is not without precedent; Wang et al. reported results showing that further increasing  $\tilde{b}_H$  beyond the point of full encapsulation of the micelle by the hydrophilic shell has the sole effect of increasing the shell thickness<sup>70</sup>.

#### 4. CONCLUSIONS

This investigation has highlighted the importance of the parameter  $\mathcal{R}_l$ , representing the lipophilic-fluorophilic block length ratio, in the self-assembly of linear BAC triblock copolymers in multicompartment micelles. A morphological deviation from “onion-like” micelle morphologies is observed to occur in BAC-based systems at high lipophilic-fluorophilic ratios: in

contrast to ABC micelles retaining a layered structure, BAC micelles exhibit a structural inversion, adopting a structure with a dominant lipophilic core and fluorophilic patches.

The structures adopted by micelles composed of linear BAC triblock copolymers are well described by a horseshoe-like diagram, as seen in Figures 5-8. Although regimes I and III exist at far ends of the  $\mathcal{R}_l$  spectrum, their structures are strikingly similar, both possessing a core composed of either the lipophilic or the fluorophilic species, whichever is dominant; the deficient species forms patches surrounding the core, while both regimes retain a hydrophilic corona. Regime II, by contrast, displays markedly different structure from either extreme, with multi-cored structures being preferred over single-cored spheroids.

For systems of triblock copolymers with bulky side chains, intuition suggests that there exists a natural extension of the structural parameter  $\mathcal{R}_l$  into a more general form  $\mathcal{R}$  which does not require the aforementioned assumption of copolymer linearity. Precise determination of the mechanistic relationship between block copolymer architecture and micelle structure is the focus of ongoing study by the authors. Nonetheless, for systems where the assumption of copolymer linearity is applicable, the lipophilic-fluorophilic block length ratio is clearly an important controlling factor in the resultant micelle morphology. As such, the parameter  $\mathcal{R}_l$  serves as an excellent predictive control parameter of micelle structure in linear BAC triblock copolymer systems.

## 5. ACKNOWLEDGEMENTS

This research was supported by the U.S. Department of Energy, Office of Science, Office of Basic Energy Sciences, under Award DE-FG02-03ER15459.

## 6. REFERENCES

1. Trost, B. M. The Atom Economy--a Search for Synthetic Efficiency. *Science* **1991**, *254*, 1471-1477.
2. Trost, B. M. Atom Economy—a Challenge for Organic Synthesis: Homogeneous Catalysis Leads the Way. *Angew. Chem. Int. Ed.* **1995**, *34*, 259-281.
3. Sheldon Roger, A. Atom Efficiency and Catalysis in Organic Synthesis. *Pure Appl. Chem.* **2000**, *72*, 1233-1246.
4. McCarroll, A. J.; Walton, J. C. Programming Organic Molecules: Design and Management of Organic Syntheses through Free-Radical Cascade Processes. *Angew. Chem. Int. Ed.* **2001**, *40*, 2224-2248.
5. Lam, A. Y. S.; Li, V. O. K. Chemical-Reaction-Inspired Metaheuristic for Optimization. *EEE Trans. Evol. Comput.* **2010**, *14*, 381-399.
6. Lam, A. Y. S.; Li, V. O. K. Chemical Reaction Optimization: A Tutorial. *Memet. Comput.* **2012**, *4*, 3-17.
7. Szeto, W. Y.; Wang, Y.; Wong, S. C. The Chemical Reaction Optimization Approach to Solving the Environmentally Sustainable Network Design Problem. *Comput. Aided Civ. Inf. Eng.* **2014**, *29*, 140-158.
8. Winnacker, M.; Vagin, S.; Rieger, B. Cooperative Catalysis in Polymerization Reactions. In *Cooperative Catalysis: Designing Efficient Catalysts for Synthesis*, 2015.
9. Madhavan, N.; Jones, C. W.; Weck, M. Rational Approach to Polymer-Supported Catalysts: Synergy between Catalytic Reaction Mechanism and Polymer Design. *Acc. Chem. Res.* **2008**, *41*, 1153-1165.
10. Weck, M.; Jones, C. W. Mizoroki–Heck Coupling Using Immobilized Molecular Precatalysts: Leaching Active Species from Pd Pincers, Entrapped Pd Salts, and Pd Nhc Complexes. *Inorg. Chem.* **2007**, *46*, 1865-1875.
11. Long, W. Designing Immobilized Catalysts for Chemical Transformations: New Platforms to Tune the Accessibility of Active Sites. Dissertation, Georgia Institute of Technology, Atlanta, 2012.
12. End, N.; Schöning, K.-U. Immobilized Catalysts in Industrial Research and Application. In *Immobilized Catalysts: Solid Phases, Immobilization and Applications*, Kirschning, A., Ed. Springer-Verlag: Berlin, 2004; Vol. 242.
13. Trapp, O.; Troendlin, J. Studies of Immobilized Catalysts. In *Molecular Catalysts: Structure and Functional Design*, Gade, L. H.; Hofmann, P., Eds. Wiley-VCH: 2014.
14. Hübner, S.; de Vries, J. G.; Farina, V. Why Does Industry Not Use Immobilized Transition Metal Complexes as Catalysts? *Adv. Synth. Catal.* **2016**, *358*, 3-25.
15. Cozzi, F. Immobilization of Organic Catalysts: When, Why, and How. *Adv. Synth. Catal.* **2006**, *348*, 1367-1390.
16. Sabater, S.; Mata, J. A.; Peris, E. Catalyst Enhancement and Recyclability by Immobilization of Metal Complexes onto Graphene Surface by Noncovalent Interactions. *ACS Catal.* **2014**, *4*, 2038-2047.
17. Huang, H.; Denard, C. A.; Alamillo, R.; Crisci, A. J.; Miao, Y.; Dumesic, J. A.; Scott, S. L.; Zhao, H. Tandem Catalytic Conversion of Glucose to 5-Hydroxymethylfurfural with an Immobilized Enzyme and a Solid Acid. *ACS Catal.* **2014**, *4*, 2165-2168.
18. Lohr, T. L.; Marks, T. J. Orthogonal Tandem Catalysis. *Nat. Chem.* **2015**, *7*, 477.
19. Rosser, T. E.; Reisner, E. Understanding Immobilized Molecular Catalysts for Fuel-Forming Reactions through Uv/Vis Spectroelectrochemistry. *ACS Catal.* **2017**, *7*, 3131-3141.

20. Bullock, R. M.; Das, A. K.; Appel, A. M. Surface Immobilization of Molecular Electrocatalysts for Energy Conversion. *Chem. Eur. J* **2017**, *23*, 7626-7641.
21. Song, C. E.; Yang, J. W.; Roh, E. J.; Lee, S. g.; Ahn, J. H.; Han, H. Heterogeneous Pd-Catalyzed Asymmetric Allylic Substitution Using Resin-Supported Trost-Type Bisphosphane Ligands. *Angew. Chem. Int. Ed.* **2002**, *41*, 3852-3854.
22. Annis, D. A.; Jacobsen, E. N. Polymer-Supported Chiral Co(Salen) Complexes: Synthetic Applications and Mechanistic Investigations in the Hydrolytic Kinetic Resolution of Terminal Epoxides. *J. Am. Chem. Soc.* **1999**, *121*, 4147-4154.
23. Peukert, S.; Jacobsen, E. N. Enantioselective Parallel Synthesis Using Polymer-Supported Chiral Co(Salen) Complexes. *Org. Lett.* **1999**, *1*, 1245-1248.
24. Chapuis, C.; Barthe, M.; de Saint Laumer, J. Y. Synthesis of Citronellal by Rhi-Catalysed Asymmetric Isomerization of N,N-Diethyl-Substituted Geranyl- and Nerylamines or Geraniol and Nerol in the Presence of Chiral Diphosphino Ligands, under Homogeneous and Supported Conditions. *Helv. Chim. Acta* **2001**, *84*, 230-242.
25. Poli, R. Site Isolation for Non-Orthogonal Tandem Catalysis in Confined Nanospaces. In *Effects of Nanoconfinement on Catalysis*, Poli, R., Ed. Springer International Publishing: Cham, 2017; pp 209-258.
26. Fukuzumi, S.; Lee, Y. M.; Nam, W. Immobilization of Molecular Catalysts for Enhanced Redox Catalysis. *ChemCatChem* **2018**, *10*, 1686-1702.
27. Yang, H.; Fu, L.; Wei, L.; Liang, J.; Binks, B. P. Compartmentalization of Incompatible Reagents within Pickering Emulsion Droplets for One-Pot Cascade Reactions. *J. Am. Chem. Soc.* **2015**, *137*, 1362-1371.
28. Dydio, P.; Ploeger, M.; Reek, J. N. H. Selective Isomerization–Hydroformylation Sequence: A Strategy to Valuable A-Methyl-Branched Aldehydes from Terminal Olefins. *ACS Catal.* **2013**, *3*, 2939-2942.
29. Lu, J.; Dimroth, J.; Weck, M. Compartmentalization of Incompatible Catalytic Transformations for Tandem Catalysis. *J. Am. Chem. Soc.* **2015**, *137*, 12984-12989.
30. Jain, S.; Zheng, X.; Jones, C. W.; Weck, M.; Davis, R. J. Importance of Counterion Reactivity on the Deactivation of Co–Salen Catalysts in the Hydrolytic Kinetic Resolution of Epichlorohydrin. *Inorg. Chem.* **2007**, *46*, 8887-8896.
31. Hopwood, D. A.; Sherman, D. H. Molecular Genetics of Polyketides and Its Comparison to Fatty Acid Biosynthesis. *Annu. Rev. Genet* **1990**, *24*, 37-62.
32. Arigoni, D.; Sagner, S.; Latzel, C.; Eisenreich, W.; Bacher, A.; Zenk, M. H. Terpenoid Biosynthesis from 1-Deoxy-D-Xylulose in Higher Plants by Intramolecular Skeletal Rearrangement. *Proc. Natl. Acad. Sci. U.S.A* **1997**, *94*, 10600-10605.
33. Agapakis, C. M.; Boyle, P. M.; Silver, P. A. Natural Strategies for the Spatial Optimization of Metabolism in Synthetic Biology. *Nat. Chem. Biol.* **2012**, *8*, 527.
34. Shi, J.; Zhang, L.; Jiang, Z. Facile Construction of Multicompartment Multienzyme System through Layer-by-Layer Self-Assembly and Biomimetic Mineralization. *ACS Appl. Mater. Interfaces* **2011**, *3*, 881-889.
35. Miller, A. L., II; Bowden, N. B. A Materials Approach to the Dual-Site Isolation of Catalysts Bonded to Linear Polymers and Small, Ionic Molecules for Use in One-Pot Cascade Reactions. *Adv. Mater.* **2008**, *20*, 4195-4199.
36. Hartley, G. S. *Aqueous Solutions of Paraffin-Chain Salts; a Study in Micelle Formation*; Hermann & Cie: Paris, 1936.

37. Slomkowski, S., et al. Terminology of Polymers and Polymerization Processes in Dispersed Systems. *Pure Appl. Chem.* **2011**, *83*, 2229.
38. Laschewsky, A. Polymerized Micelles with Compartments. *Curr. Opin. Colloid Interface Sci.* **2003**, *8*, 274-281.
39. Lutz, J. F.; Laschewsky, A. Multicompartment Micelles: Has the Long-Standing Dream Become a Reality? *Macromol. Chem. Phys.* **2005**, *206*, 813-817.
40. Kubowicz, S.; Baussard, J. F.; Lutz, J. F.; Thünemann, A. F.; von Berlepsch, H.; Laschewsky, A. Multicompartment Micelles Formed by Self-Assembly of Linear Abc Triblock Copolymers in Aqueous Medium. *Angew. Chem. Int. Ed.* **2005**, *44*, 5262-5265.
41. Li, Z.; Kesselman, E.; Talmon, Y.; Hillmyer, M. A.; Lodge, T. P. Multicompartment Micelles from Abc Miktoarm Stars in Water. *Science* **2004**, *306*, 98-101.
42. Moughton, A. O.; Hillmyer, M. A.; Lodge, T. P. Multicompartment Block Polymer Micelles. *Macromolecules* **2012**, *45*, 2-19.
43. Moughton, A. O.; Sagawa, T.; Yin, L.; Lodge, T. P.; Hillmyer, M. A. Multicompartment Micelles by Aqueous Self-Assembly of M-a(Bc)N Miktobrush Terpolymers. *ACS Omega* **2016**, *1*, 1027-1033.
44. Lal, M.; Kumar, N. D.; Joshi, M. P.; Prasad, P. N. Polymerization in a Reverse Micelle Nanoreactor: Preparation of Processable Poly(P-Phenylenevinylene) with Controlled Conjugation Length. *Chem. Mater.* **1998**, *10*, 1065-1068.
45. Vriezema, D. M.; Comellas Aragonès, M.; Elemans, J. A. A. W.; Cornelissen, J. J. L. M.; Rowan, A. E.; Nolte, R. J. M. Self-Assembled Nanoreactors. *Chem. Rev.* **2005**, *105*, 1445-1490.
46. Peters, R. J. R. W.; Louzao, I.; van Hest, J. C. M. From Polymeric Nanoreactors to Artificial Organelles. *Chem. Sci.* **2012**, *3*, 335-342.
47. Adıgüzel, R.; Taşcıoğlu, S. Micelle Nano-Reactors as Mediators of Water-Insoluble Ligand Complexation with Cu(II) Ions in Aqueous Medium. *Chem. Pap.* **2013**, *67*, 456-463.
48. Boucher-Jacobs, C.; Rabnawaz, M.; Katz, J. S.; Even, R.; Guironnet, D. Encapsulation of Catalyst in Block Copolymer Micelles for the Polymerization of Ethylene in Aqueous Medium. *Nat. Commun.* **2018**, *9*, 841.
49. Marguet, M.; Bonduelle, C.; Lecommandoux, S. Multicompartmentalized Polymeric Systems: Towards Biomimetic Cellular Structure and Function. *Chem. Soc. Rev.* **2013**, *42*, 512-529.
50. Fischlechner, M.; Schaerli, Y.; Mohamed, M. F.; Patil, S.; Abell, C.; Hollfelder, F. Evolution of Enzyme Catalysts Caged in Biomimetic Gel-Shell Beads. *Nat. Chem.* **2014**, *6*, 791.
51. Longstreet, A. R.; McQuade, D. T. Organic Reaction Systems: Using Microcapsules and Microreactors to Perform Chemical Synthesis. *Acc. Chem. Res.* **2013**, *46*, 327-338.
52. Chou, S.-H.; Tsao, H.-K.; Sheng, Y.-J. Morphologies of Multicompartment Micelles Formed by Triblock Copolymers. *J. Chem. Phys.* **2006**, *125*, 194903.
53. Hoogerbrugge, P. J.; Koelman, J. M. V. A. Simulating Microscopic Hydrodynamic Phenomena with Dissipative Particle Dynamics. *EPL* **1992**, *19*, 155.
54. Koelman, J. M. V. A.; Hoogerbrugge, P. J. Dynamic Simulations of Hard-Sphere Suspensions under Steady Shear. *EPL* **1993**, *21*, 363.
55. Español, P.; Warren, P. B. Statistical Mechanics of Dissipative Particle Dynamics. *EPL* **1995**, *30*, 191.
56. Groot, R. D.; Warren, P. B. Dissipative Particle Dynamics: Bridging the Gap between Atomistic and Mesoscopic Simulation. *J. Chem. Phys.* **1997**, *107*, 4423-4435.

57. Zhao, Y.; Liu, Y.-T.; Lu, Z.-Y.; Sun, C.-C. Effect of Molecular Architecture on the Morphology Diversity of the Multicompartment Micelles: A Dissipative Particle Dynamics Simulation Study. *Polymer* **2008**, *49*, 4899-4909.
58. Marsat, J.-N.; Heydenreich, M.; Kleinpeter, E.; von Berlepsch, H.; Böttcher, C.; Laschewsky, A. Self-Assembly into Multicompartment Micelles and Selective Solubilization by Hydrophilic–Lipophilic–Fluorophilic Block Copolymers. *Macromolecules* **2011**, *44*, 2092-2105.
59. Gröschel, A. H.; Schacher, F. H.; Schmalz, H.; Borisov, O. V.; Zhulina, E. B.; Walther, A.; Müller, A. H. E. Precise Hierarchical Self-Assembly of Multicompartment Micelles. *Nat. Commun.* **2012**, *3*.
60. Wang, L.; Lin, J. Discovering Multicore Micelles: Insights into the Self-Assembly of Linear A-b-c Terpolymers in Midblock-Selective Solvents. *Soft Matter* **2011**, *7*, 3383-3391.
61. Zhong, C.; Liu, D. Understanding Multicompartment Micelles Using Dissipative Particle Dynamics Simulation. *Macromol. Theory Simul.* **2007**, *16*, 141-157.
62. Xia, J.; Zhong, C. Dissipative Particle Dynamics Study of the Formation of Multicompartment Micelles from A-b-c Star Triblock Copolymers in Water. *Macromol. Rapid Commun.* **2006**, *27*, 1110-1114.
63. Procházka, K.; Martin, T. J.; Webber, S. E.; Munk, P. Onion-Type Micelles in Aqueous Media. *Macromolecules* **1996**, *29*, 6526-6530.
64. Talingting, M. R.; Munk, P.; Webber, S. E.; Tuzar, Z. Onion-Type Micelles from Polystyrene-Block-Poly(2-Vinylpyridine) and Poly(2-Vinylpyridine)-Block-Poly(Ethylene Oxide). *Macromolecules* **1999**, *32*, 1593-1601.
65. Pleštil, J.; Kříž, J.; Tuzar, Z.; Procházka, K.; Melnichenko, Y. B.; Wignall, G. D.; Talingting, M. R.; Munk, P.; Webber, S. E. Small-Angle Neutron Scattering Study of Onion-Type Micelles. *Macromol. Chem. Phys.* **2001**, *202*, 553-563.
66. Read, E. S.; Armes, S. P. Recent Advances in Shell Cross-Linked Micelles. *ChemComm* **2007**, 3021-3035.
67. Synatschke, C. V., et al. Multicompartment Micelles with Adjustable Poly(Ethylene Glycol) Shell for Efficient in Vivo Photodynamic Therapy. *ACS Nano* **2014**, *8*, 1161-1172.
68. *Materials Studio*, v. 5.0; Accelrys, Inc.: San Diego, 2009.
69. Callaway, C. P.; Hendrickson, K.; Bond, N.; Lee, S.; Sood, P.; Jang, S. S. Molecular Modeling Approach to Determine the Flory-Huggins Interaction Parameter for Polymer Miscibility Analysis. *ChemPhysChem* **2018**.
70. Wang, X.; Gao, J.; Wang, Z.; Xu, J.; Li, C.; Sun, S.; Hu, S. Dissipative Particle Dynamics Simulation on the Self-Assembly and Disassembly of Ph-Sensitive Polymeric Micelle with Coating Repair Agent. *Chem. Phys. Lett.* **2017**, *685*, 328-337.

**Table 1.** Repulsion parameters  $a_{ij}$  between each pair of species in the DPD simulation system. Note that  $a_{ii} = 25.0$  by definition<sup>56</sup> [see equation (2)]. Values in shaded cells are implied by other cells due to the fact that  $a_{ij} = a_{ji}$

	<b>Block A</b>	<b>Block B</b>	<b>Block C</b>	<b>Water</b>
<b>Block A</b>	25.0	37.5	57.5	27.5
<b>Block B</b>	37.5	25.0	40.0	47.5
<b>Block C</b>	57.5	40.0	25.0	60.0
<b>Water</b>	27.5	47.5	60.0	25.0

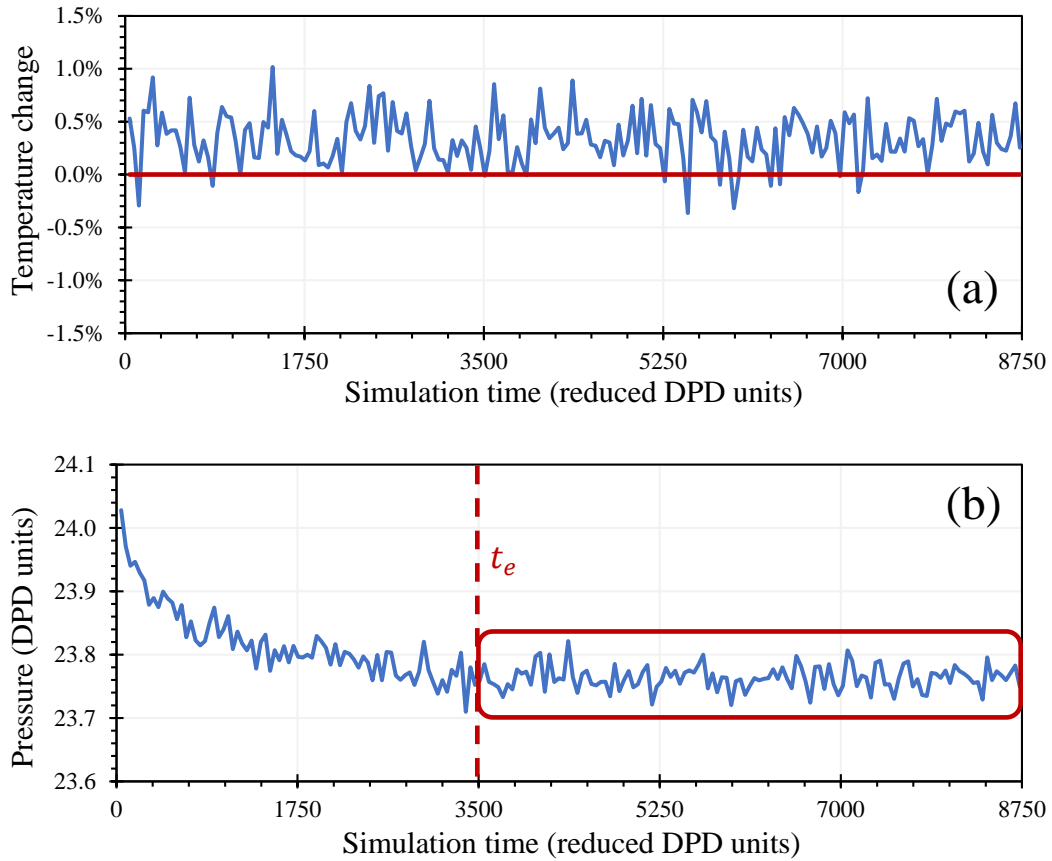


**Figure 1.** Change in (a) system temperature and (b) system pressure for a representative DPD simulation as a function of simulation time. The variation in temperature reveals an acceptably small average deviation from equipartition of approximately 0.3%, while the variation in pressure gives  $t_e = 3 \times 10^3$  reduced DPD units.

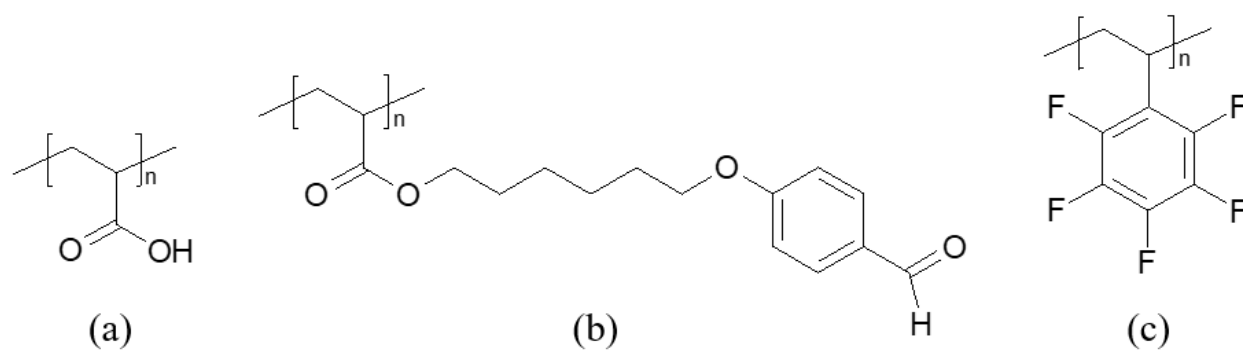


**Figure 2.** Chemical structures of blocks exhibiting (a) hydrophilic, (b) lipophilic, and (c) fluorophilic characteristics. Preliminary simulations were performed on these species to determine representative  $\chi_{ij}$ -values, which were then adjusted to ensure microphase separation between all species present in the DPD simulations.

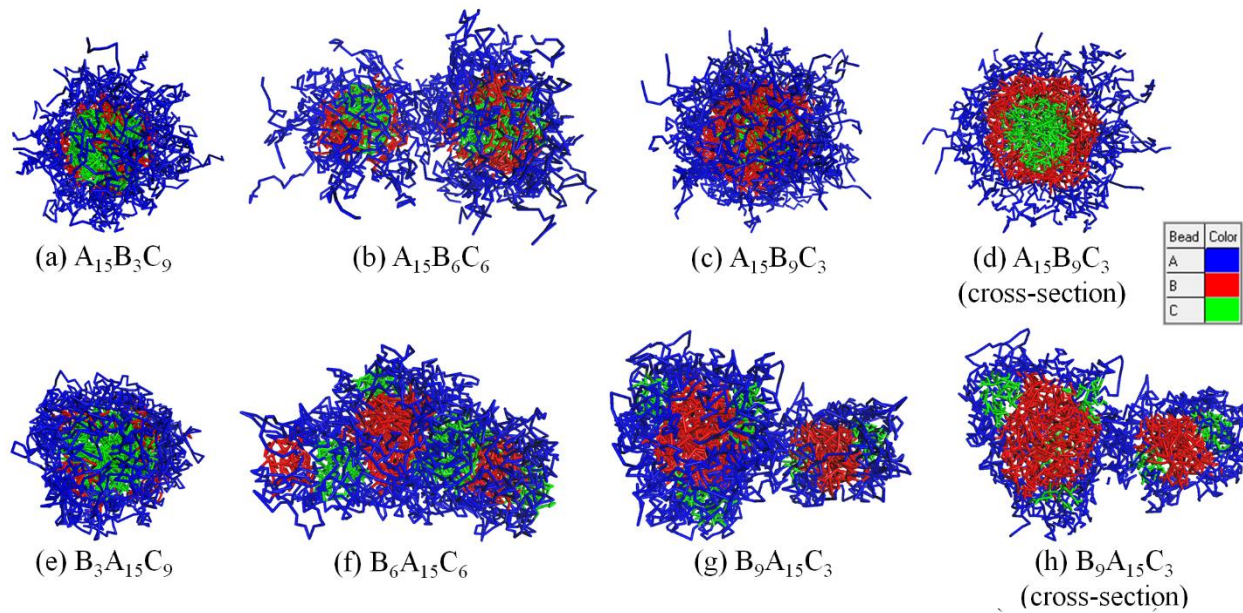


**Figure 3.** Morphological differences between (a-d) ABC and (e-h) BAC micelle systems as a function of  $\mathcal{R}_l$ . The reduced hydrophilic block length is held constant at  $\tilde{b}_H = 15$ . As seen in the cross-sectional views in (d) and (h), the two systems result in markedly different micelle structures for  $\mathcal{R}_l$ -values much greater than unity.

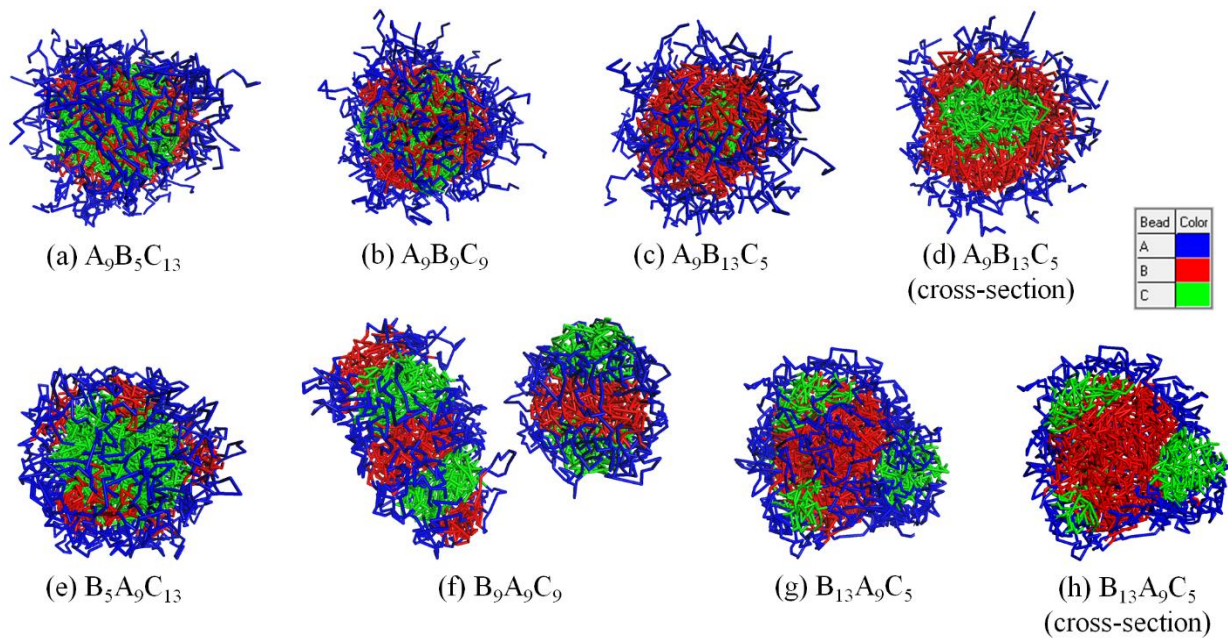


**Figure 4.** Morphological differences between (a-d) ABC and (e-h) BAC micelle systems as a function of  $\mathcal{R}_l$ . The reduced hydrophilic block length is held constant at  $\tilde{b}_H = 9$ .

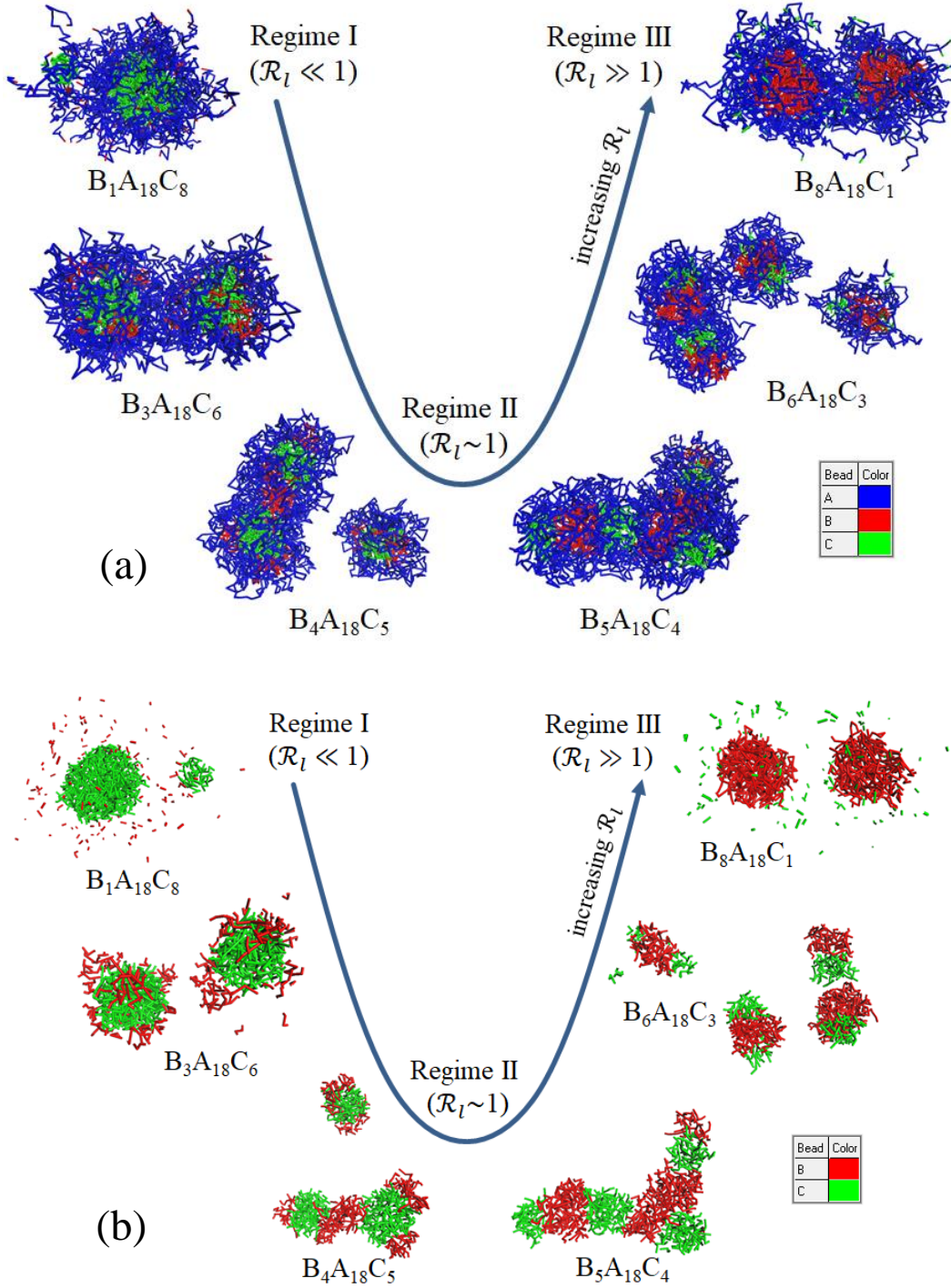


**Figure 5.** (a) A horseshoe diagram demonstrating the structural variation of a hydrophilic-rich ( $\tilde{b}_H = 18$ ) BAC micelle as a function of  $\mathcal{R}_l$ . Regimes I and III display striking morphological similarities, highlighting the importance of  $\mathcal{R}_l$  as a governing structural parameter. (b) A horseshoe diagram of the same system with hydrophilic-block visibility disabled. Water visibility is disabled in both cases for clarity.

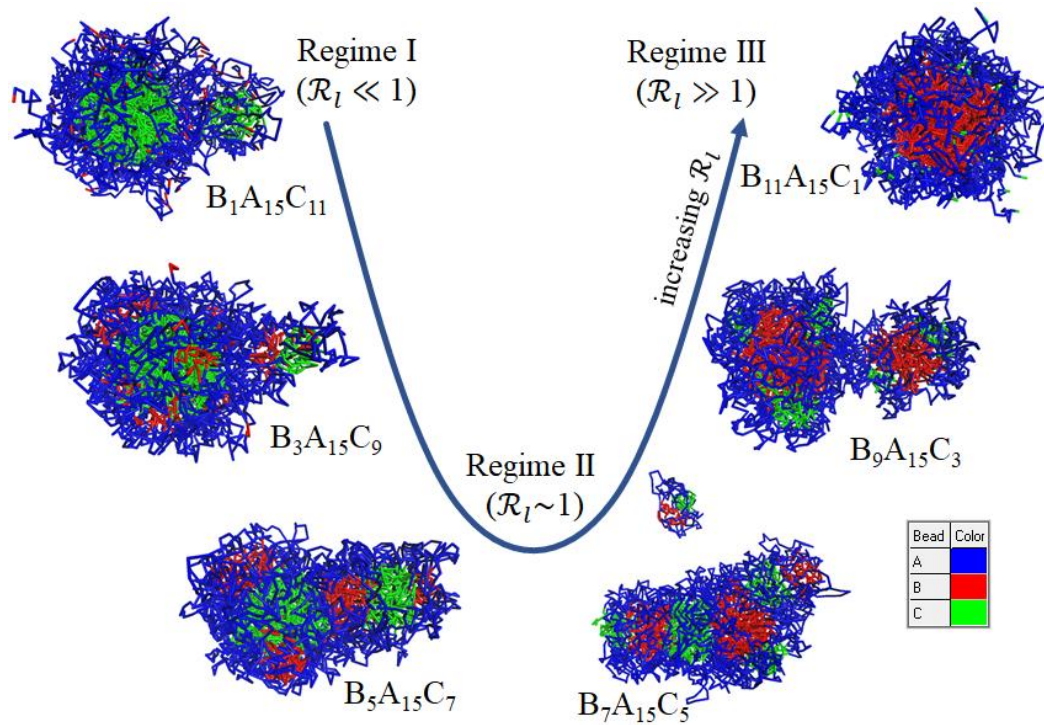


**Figure 6.** A horseshoe diagram demonstrating the structural variation of a BAC micelle with  $\tilde{b}_H = 15$  as a function of  $\mathcal{R}_l$ . Water visibility is disabled for clarity.

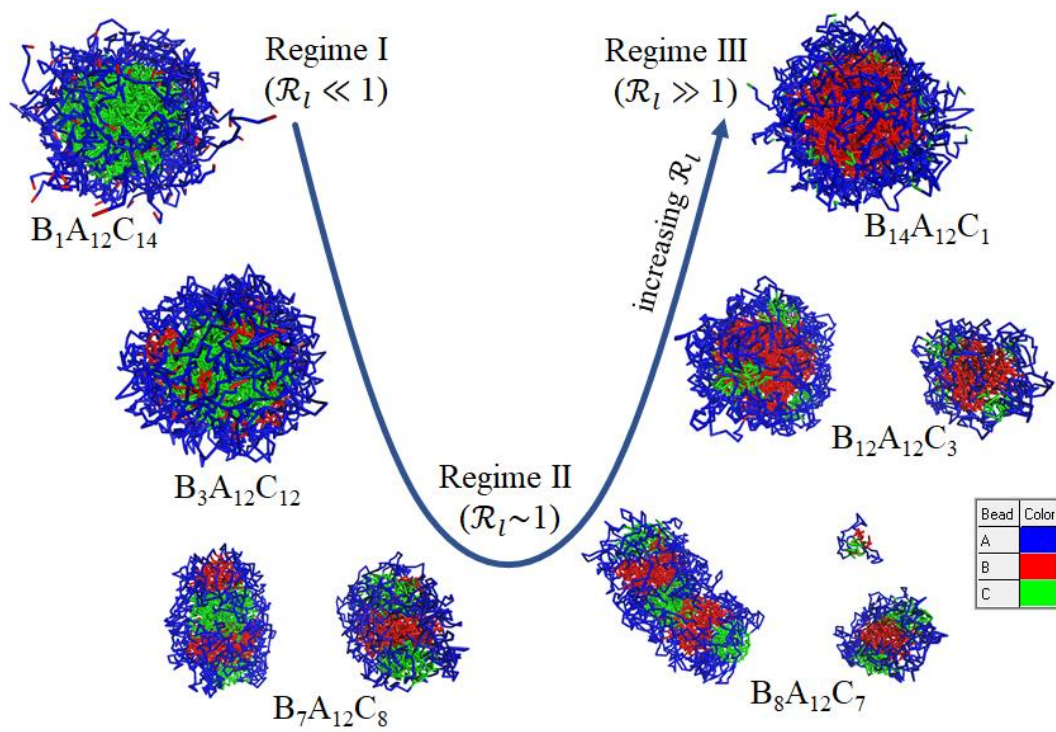


**Figure 7.** A horseshoe diagram demonstrating the structural variation of a BAC micelle with  $\tilde{b}_H = 12$  as a function of  $\mathcal{R}_l$ . Water visibility is disabled for clarity.

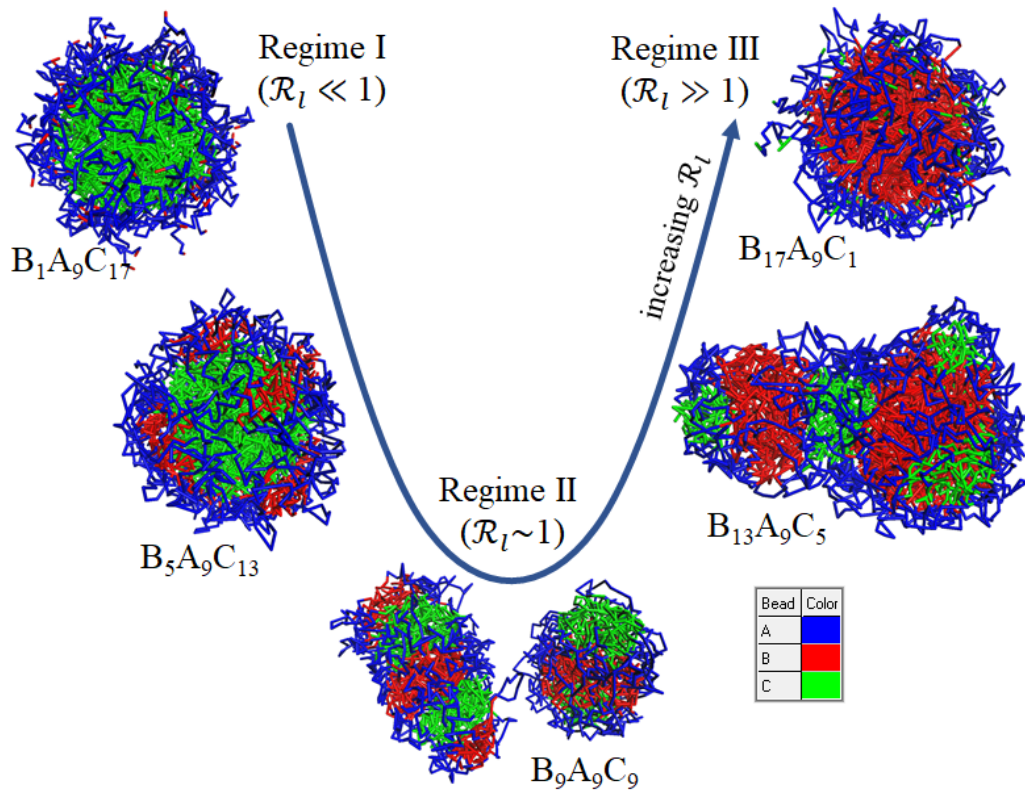


**Figure 8.** A horseshoe diagram demonstrating the structural variation of a relatively hydrophilic-poor ( $\tilde{b}_H = 9$ ) BAC micelle as a function of  $\mathcal{R}_l$ . Water visibility is disabled for clarity.

## TOC Graphics

